Sensors & Actuators: B. Chemical 309 (2020) 127728

Contents lists available at ScienceDirect

Sensors and Actuators B: Chemical

journal homepage: www.elsevier.com/locate/snb

A sensitive lateral flow immunochromatographic strip with prussian blue nanoparticles mediated signal generation and cascade amplification

Meiling Tian[a], Wenyue Xie[a], Ting Zhang[a], Yang Liu[b], Zhisong Lu[a], Chang Ming Li[a], Yingshuai Liu[a,*]

[a] Institute for Clean Energy and Advanced Materials, School of Materials and Energy, Southwest University, Chongqing, 400715, PR China
[b] Institute of Food Science and Technology, Chinese Academy of Agricultural Sciences / Key Laboratory of Agro-Products Processing, Ministry of Agriculture, No.1 Nongda South Road, Xibeiwang, Haidian District, Beijing, 100193, PR China

ARTICLE INFO

Keywords:
Immunochromatography
Signal amplification
Prussian blue nanoparticle
Colorimetric assay

ABSTRACT

This work reports a low-cost, fast and highly sensitive lateral flow immunoassay (LFIA) platform with Prussian blue nanoparticle (PBNP) as a new reporter, which efficiently mediates an on-demand cascade signal amplification by catalyzing oxidation of chromogenic reagent 3,3′,5,5′-tetramethylbenzidine (TMB). In this case, PBNPs are accumulated on the test line through the specific immune interaction, resulting in a blue-colored line. The colorimetric signal can be further amplified via the peroxidase mimic PBNP-catalyzed TMB oxidation to produce an insoluble blue-violet precipitate. Under an optimal condition, a limit of detection (LOD) at 10 pg $mL^{-1}$is achieved for rabbit IgG (RIgG) detection, which is 2–3 orders of magnitude better than the conventional LFIA strip using colloidal gold nanoparticle as a label. A macromolecular RIgG and a small molecular mycotoxin ochratoxin A (OTA) are also successfully analyzed in mimicking samples, demonstrating its good practicability of the proposed platform in a variety of fields.

1. Introduction

Enzyme-linked immunosorbent assay (ELISA) as one of the most popular analytical platform has been widely utilized in many fields such as clinical diagnostics, food safety, and fundamental research [1,2]. However, its practicability in real-time and on-site analysis is greatly limited because of the tedious and time-consuming protocols, as well as its strong dependence on professional operator [3]. Lateral flow immunoassay (LFIA) is a novel analytical approach with many merits including low cost, fast response, easy-to-use, and high throughput capability [4,5]. More importantly, the LFIA strip is well suitable for on-site fast screening of diseases and food contamination in rural areas with poor resources [6].

Despite of the above mentioned merits, the poorer sensitivity of the LFIA strip compared with other immunoassay platforms severely limits its practical applications in different fields. Much effort has been devoted to improve its sensitivity in the past years. Natural bioenzymes (such as horseradish peroxidase) conjugated gold nanoparticle (AuNP) has been constructed and employed to improve LFIA sensitivity via catalytic signal amplification [7]. Unfortunately, natural bioenzymes are very expensive and easy to be denatured. Alternatively, many kinds of nanomaterials including Fe_3O_4 NP, Fe_2O_3@Au core-shell NP, Au-Ag NP, quantum dots (QDs) integrated fluorescent nanospheres (FNs) are employed as reporters to improve the performance of the LFIA strips [8–10]. These strategies, however, still face some challenges such as long preparation time, sophisticated synthesis, requirement of large and expensive instrumentation, limiting their further application in LFIA. Therefore, it is highly desirable for a novel labeling tag, which can be easily synthesized and possesses unique physico/chemical properties for both signal generation and amplification.

Prussian blue nanoparticle (PBNP) has been attracting extensive attention from biomedical researchers because of its favorable biocompatibility and unique properties such as low cost, high surface-to-volume ratio, ease of synthesis and surface modification [11–14]. In view of these excellent properties, PBNPs have been used as a drug carrier [15], imaging contrast agents and therapeutic hyperthermia agents [16]. Furthermore, PBNPs are demonstrated to have intrinsic peroxidase-like activity and have been used as labels to establish electrochemical and optical bio-/chemical sensors [17–20].

Inspired by these previous investigations, PBNP instead of AuNP is used in this work as a new labeling tag for both signal generation and on-demand cascade amplification. The LFIA sensitivity can be significantly improved by the PBNP tag, overcoming the above mentioned drawbacks of natural bioenzymes and sophisticated nanomaterials. A

* Corresponding author.
E-mail address: ysliu@swu.edu.cn (Y. Liu).

https://doi.org/10.1016/j.snb.2020.127728
Received 24 September 2019; Received in revised form 20 December 2019; Accepted 14 January 2020
Available online 27 January 2020

signal generation is accomplished by the aggregation of the blue-colored PBNPs, resulting in a visual test line. A further signal amplification can be easily realized based on the peroxidase mimic PBNP-catalyzed TMB oxidation. The test line is significantly deepened because of the PBNP-catalyzed cascade production of the insoluble blue-violet oxidized TMB (Ox-TMB). A protein analyte RIgG and a small target mycotoxin OTA were successfully analyzed by the developed PBNP-based LFIA strip based on sandwich and competitive immunoassay, respectively.

2. Experimental

2.1. Chemical and reagents

$FeCl_3{\cdot}6H_2O$, $K_4[Fe(CN)_6]{\cdot}3H_2O$, $Na_2HPO_4{\cdot}12H_2O$, $NaH_2PO_4{\cdot}2H_2O$, citric acid, N-(3-Dimethylaminopropyl)-N'-carbodiimide hydrochloride (EDC), N-hydroxysulfosuccinimide(sulfo-NHS), bovine serum albumin (BSA), Ochratoxin A(OTA), and sucrose (Suc) were received from Aladdin (Shanghai, China). Goat anti-RIgG (Ab_2) and RIgG were bought from Sigma-Aldrich (Shanghai, China). Anti-RIgG produced in mouse (Ab_1) was provided by Bioss (Beijing, China). OTA-BSA and anti-OTA monoclonal antibody (Ab_3) were purchased Shenzhen Anti Biotechnology Co., Ltd (Shenzhen, China). TMB for blotting was obtained from Nanjing Institute of Bioengineering (Nanjing, China). Nitrocellulose (NC) membrane, glass fiber, adsorbent pad and PVC backing card were bought from Shanghai Kinbio Tech (Shanghai, China).

2.2. Preparation of PBNPs and PBNP-Ab2 conjugates

PBNPs were synthesized according to the methods described previously [21,22]. In short, 98 mg of citric acid was dissolved in 1 mM $K_4[Fe(CN)_6]$ aqueous solution (20 mL) and 1 mM $FeCl_3$ solution (20 mL), respectively. After heating to 60℃, these two solutions were quickly mixed and vigorously stirred for 3 min, resulting a blue dispersion, which was continuously stirred until cooled to room temperature.

Ab_2 was conjugated to the PBNPs via the EDC/NHS coupling method. Specifically, 4 mL PBNP solution was centrifuged at 14500 rpm for 25 min, followed by redispersion in 4 mL of 0.05 M phosphate buffer (PB; 0.05 M Na_2HPO_4/ NaH_2PO_4, pH 7.4). 16 mg EDC and 32 mg sulfo-NHS were added into the above solution to activate the carboxyl group on PBNP surface. 10 μL of Ab_2 was then dropped into the activated PBNP solution. The mixture was incubated for 2 h at 37℃ under gentle mechanical oscillation, followed by passivation with 1 % (m/V) BSA in PB. After three-time washing, the resulted PBNP-Ab_2 was redispersed in 800 μL PBS containing 1 % BSA and 1 % Suc.

2.3. Fabrication of LFIA strip

Scheme 1 shows the structure of the LFIA strip. Antibody dispensing, membrane blocking, and assembly of each part were carried out according to our previous work [23].

2.4. Optimization of the assay conditions for LFIA strip

First, the reaction time between RIgG and the PBNP-Ab_2 was optimized. 100 μL of 100 ng mL^{-1} RIgG in PBS and 20 μL of PBNP-Ab_2 were mixed and incubated for 5 min, 10 min, 15 min, 20 min, 25 min, and 30 min, respectively, and then the mixture was dispensed on the sample pad. After 30 min, the strips were imaged with a smart phone. Grey intensity of the test line was analyzed by the free software imageJ.

In order to obtain a good signal-to-noise ratio, it is critical to optimize the amount of PBNP-Ab_2 and the blocking reagent. As for the PBNP-Ab_2 optimization, 1 % BSA was used to block the nitrocellulose membrane, 5 μL, 10 μL, 15 μL and 20 μL of PBNP-Ab_2 at 0.535 mg mL^{-1} was mixed with 100 μL of 100 ng mL^{-1} RIgG in PBS respectively, while PBS without RIgG was used as a blank. As for optimization of BSA concentration, 1 %, 3 %, 5 %, 7 % and 10 % of BSA was selected to block the nitrocellulose membrane. In addition, the test strip was imaged every 3 min over the period of 3–36 min for optimization of the assay time.

2.5. RIgG and OTA detection on the LFIA strip

RIgG was diluted to desired concentrations with PBS and 10 % human serum respectively. Sandwich immunoassay was then carried out under the optimal parameters achieved in Section 2.4. After the end of TMB color development, all strips were imaged by a smart phone for quantitative analysis.

A small molecule mycotoxin OTA was also detected by the PBNP-based LFIA strip based on a competitive immunoassay. 1.4 μL of OTA-BSA at 2.0 mg mL^{-1} was immobilized on the NC membrane to make a test line. PBNP-labeled anti-OTA monoclonal antibody (PBNP-Ab_3) were mixed with OTA-spiked soybean extractives and then dispensed on the sample pad to perform the lateral flow assay.

2.6. Data analysis

Grey value from each test line was employed for further quantitative analysis. The change percentage of the grey intensity (ΔG%) was calculated according to the method reported previously [23]. A deeper color gives a bigger grey value. In order to reduce the influence of background, ΔG% was obtained on the basis of Eq. (1).

$$\Delta G\% = [(G_t - G_c)/G_c] \times 100\ \% \quad (1)$$

Where G_c is the grey value for negative control, while G_t is the grey value for test group. Thus, the more PBNPs are captured at the test zone, the color of the test line is deeper and the ΔG% is bigger.

As for competitive OTA test, the lower level of OTA is applied, the bigger grey value is obtained. Thus the calculation principle is slightly different from the above one. $\Delta G_{OTA}\%$ is calculated according to the following Eq. (2).

$$\Delta G_{OTA}\% = [(G_c - G_t)/G_c] \times 100\ \% \quad (2)$$

3. Results and discussion

3.1. Principle of the assay

As schematically illustrated in Scheme 1, PBNP-Ab_2-analyte immunocomplex moves forward along the strip and is captured by Ab_1 at the test line, resulting in a blue-colored test line. The excess PBNP-Ab_2 conjugate continuously moves forward and is then stored in the adsorbent pad. Chromogenic TMB for blotting was then added to testing zone and locally oxidized into blue colored Ox-TMB, resulting in efficient signal amplification. A qualitative evaluation can be realized with naked eyes, while a quantitative determination is accomplished by a smart phone for imaging and the free software imageJ for acquiring the grey value. Compared with the previously reported PBNP-based lateral flow assay [24], the entire preparation process of PBNP in this work can be completed in a few minutes and the resulted PBNP can be stored at 4℃ for a long time. Moreover, in this design the PBNP not only works as a reporter, but as an artificial peroxidase to catalyze cascade signal amplification without need of natural bioenzymes and sophisticated conjugation process.

3.2. Characterization of PBNP and PBNP-Ab_2

Size and zeta potential of the PBNP and PBNP-Ab_2 were measured with a dynamic light scattering (DLS) instrument (Zetasizer Nano ZS 90,

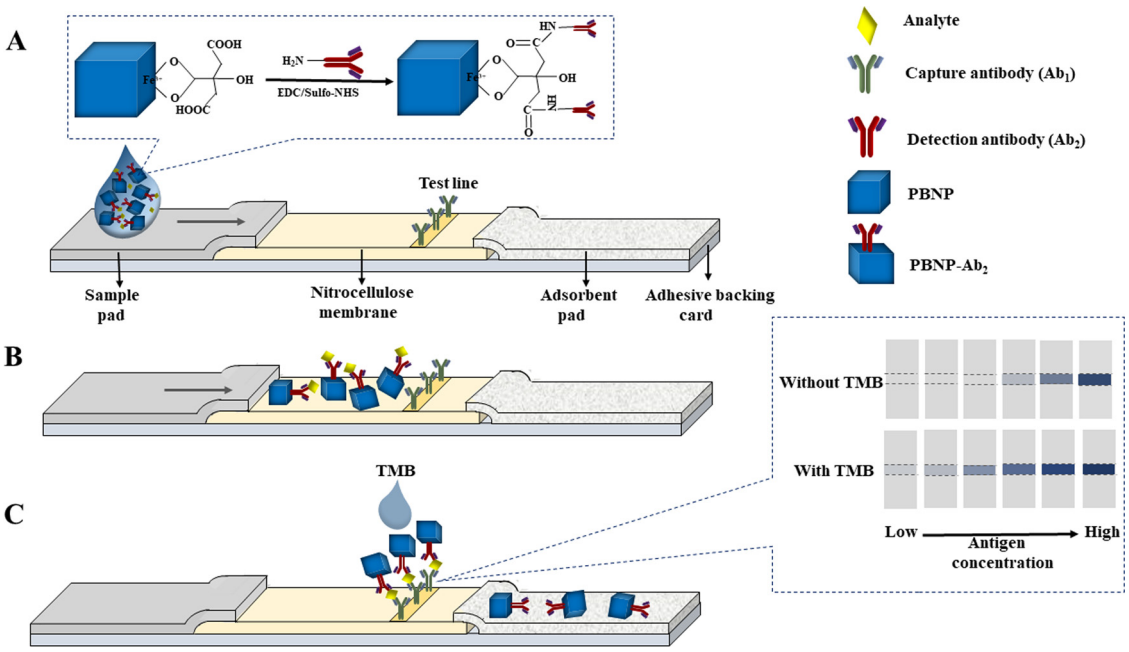

Scheme 1. Schematic illustration of the PBNP-induced signal amplification on a LFIA strip. (A) Synthesis of PBNP-Ab_2 and assembly of the lateral flow strip; (B) Capillary force-driven PBNP-Ab_2-analyte complex migration to the test line on nitrocellulose membrane; (C) PBNP-Ab_2-analyte complexes are captured by Ab_1 on test line and the excess PBNP-Ab_2 continuously migrates toward the adsorbent pad.

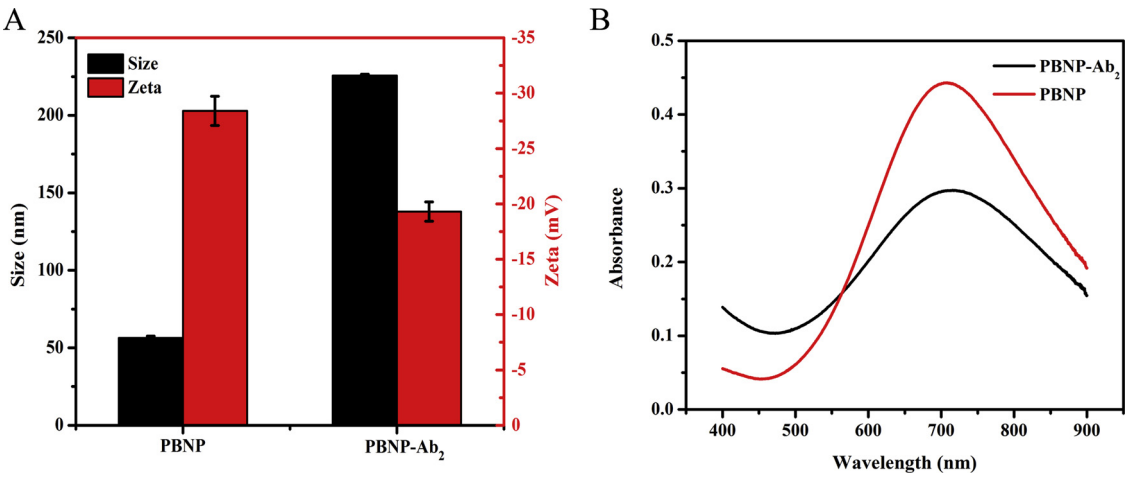

Fig. 1. Characterization of PBNP and PBNP-Ab_2. (A) Hydrodynamic diameter and zeta potential, (B) UV–vis spectra of prepared PBNP and PBNP-Ab_2.

Malvern, UK). As shown in Fig. 1A, the diameter of PBNP is around 56.36 ± 1.15 nm with polydispersity index (PDI) 0.054. The small PDI value indicates that the PBNPs have uniform size and are well dispersed in aqueous solution. The diameter of PBNP-Ab_2 significantly increases to 225.6 ± 0.91 nm with PDI 0.218. The dramatic increase in the hydrodynamic size of PBNP-Ab_2 compared with PBNP is apparently attributed to Ab_2 coating, which not only increases the size of each PBNP but results in formation of PBNP clusters due to Ab_2-induced crosslinking. Although Ab_2 coating results in significant size increase, the cluster is still dispersible in PBS and moves smoothly on the test strip. Thus the PBNP-Ab_2 conjugate is suitable for application in LFIA. Zeta potential of PBNP is −28.4 mV, which clearly results from the abundant carboxyl group (citric acid) on PBNP surface. However, zeta potential of the PBNP-Ab_2 shifts to −19.3mv after Ab_2 conjugation. A broad absorbance band from 500 nm to 900 nm is observed from UV–vis spectra of the PBNP and PBNP-Ab_2 solution in Fig. 1B. An adsorption peak at 707 nm and 716 nm is recorded from PBNP and PBNP-Ab_2, respectively. The small red shift from 707 nm to 716 nm should be attributed to Ab_2 coating on PBNP surface.

Size and morphology of the PBNP and PBNP-Ab_2 was also monitored by a transmission electron microscopy (TEM) (JEOL, JEM-2100). Fig.2A shows that the PBNPs are monodispersed cubes with narrow size distribution. An average size is about 50 nm in diameter, which is very suitable for serving as a tag in LFIA strip. Fig. 2B shows the TEM image of PBNP-Ab_2. An obvious coating layer around the PBNP is observed from the image of PBNP-Ab_2, indicating that Ab_2 is successfully coupling on PBNP surface. In comparison with the monodispersed PBNP, some PBNPs are crosslinked with each other due to the Ab_2 conjugation, resulting in some bigger clusters as shown in Fig. 2B. This result is well consistent with the larger hydrodynamic size of PBNP-Ab_2 observed in Fig. 1A.

3.3. Antibody conjugation efficiency on PBNP surface

Antibody conjugation efficiency on PBNP surface is of great importance to the performance of LFIA strip. Original Ab_2 concentration

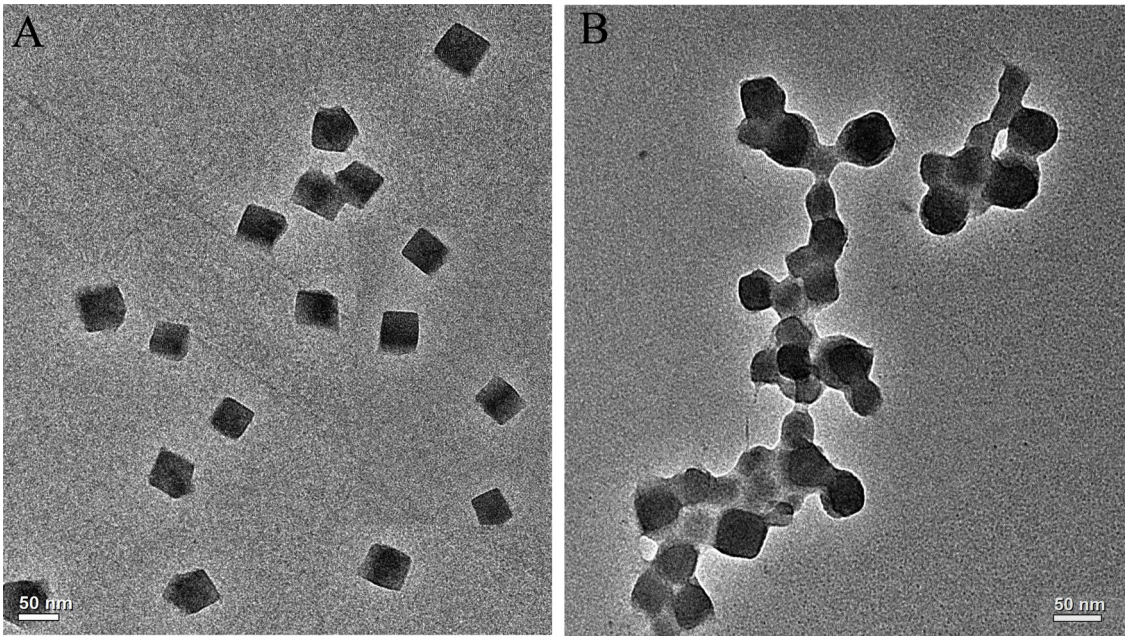

Fig. 2. TEM images of(A)PBNP and(B)PBNP-Ab_2.

and post-coupling Ab_2 concentration in supernatant was determined by measuring Ab_2 concentration using BCA protein assay kit, respectively. The coupling percentage is determined to be 76.4 % based on the calculation method of Ab_2 amount in post-coupling supernatant divided by the original Ab_2 amount. The high conjugation rate guarantees that RIgG (analyte) in sample can be efficiently captured by PBNP-Ab_2, resulting in PBNP-Ab_2-RIgG complex formation. Therefore, a visual blue band is subsequently created due to the aggregation of PBNP on the test line.

3.4. Optimization of the experimental parameters

Grey intensity of the test lines versus the incubation time of RIgG and PBNP-Ab_2 mixture was plotted in a period of 5–30 min. Fig. 3A shows that the incubation time doesn't play an obvious effect on the signal intensity. It is probably attributed to the very efficient immunoreaction between PBNP-Ab_2 and RIgG in a solution. In addition, PBNP-Ab_2-RIgG complex is continuously formed in the test strip when the mixture of PBNP-Ab_2 and RIgG moves forward. The detection procedure is accomplished by simple mixing and dropping, eliminating a complicated operation process like the conventional ELISA. In this assay, the visual test band was derived from the accumulation of PBNP-Ab_2 and subsequent TMB color development. The volume of PBNP-Ab_2 could directly affect signal intensity and assay sensitivity. As seen in Fig. 3B, ΔG% value gradually increases with the increase of PBNP-Ab_2 volume, while the highest ΔG% is observed when 15 μL PBNP-Ab_2 is applied on each strip. Further increase of PBNP-Ab_2 amount results in a significant decrease in ΔG%. It probably because that too much PBNP-Ab_2 results in a higher background and a lower ΔG%. Thus, 15 μL PBNP-Ab_2 as the best volume was applied to subsequent experiments.

In order to reduce background resulted from nonspecific adsorption of PBNP-Ab_2 and RIgG, BSA was employed as a blocking reagent to passivate any possible binding sites in the nitrocellulose membrane. BSA at different concentrations was tested in this experiment. The highest ΔG% was achieved when the concentration of BSA was 7 % (Fig. 3C). Further increase of BSA did not give better results. It is explained that higher levels of BSA hinder the flow of PBNP-Ab_2-RIgG complex in the strip and prolongs the reaction time. Therefore,7 % BSA was used as an optimal blocking reagent. Fig. 3D shows a plot of signal intensity versus the assay time from 3 to 36 min. Grey intensity of the test band gradually increases with the elongation of assay time and reach a plateau at 24 min, indicating that the immunoreaction is almost finished in 24 min. After that, the TMB was dropped on the test line for 6 min to deepen the color intensity and amplify the signal. The entire analysis can be finished in about 30 min, which is much shorter than the microtitre plate-based ELISA.

3.5. Practicability evaluation of PBNP-LFIA platform

Feasibility and superiority of the proposed LFIA platform was investigated using RIgG as a model target. RIgG at concentrations ranging from 10 pg mL^{-1} to 1 μg mL^{-1} was mixed with an equal volume of PBNP-Ab_2 solution, respectively, and then loaded onto the sample pad of each test strip. It is clearly observed from Fig. 4A that there are distinct blue bands for RIgG at 100 ng mL^{-1} and 1 μg mL^{-1} before addition of TMB for signal amplification. Only a weak band is distinguished with naked eyes when RIgG is at 10 ng mL^{-1}. However, the signal intensity of testing bands is significantly improved after PBNP-catalyzed signal amplification. A weak test band can be easily distinguished by naked eyes when RIgG concentration downs to 10 pg mL^{-1}. The strips in Fig. 4A were then quantitatively analyzed with imageJ. A statistical comparison between two data sets of blank and 10 pg mL^{-1} is performed based on their grey intensities. Statistical hypothesis testing with $p < 0.05$ indicates that 10 pg mL^{-1} is successfully detected with the proposed quantitative analysis method after the amplification. A lower concentration 1 pg mL^{-1} was also tested. As shown in Fig. 4A, the test line for 1 pg mL^{-1} is difficult to be distinguished by naked eyes from the blank group, which is also confirmed by the statistical analysis with $p > 0.05$. ΔG% values were calculated according to the Eq. 1 described in Section 2.6. Fig. 4B shows a linear relationship ($R^2 = 0.996$) plotted with double logarithmic axes over RIgG concentrations in a range of 10 pg mL^{-1} to 1 μg mL^{-1}. The lowest concentration that is distinguishable by naked eyes is 10 pg mL^{-1}, which is 2–3 orders of magnitude lower than that achieved by the traditional AuNP-based LFIA strip. RIgG spiked human serum (10 %) was also successfully analyzed by the proposed platform. As shown in Fig. 4C, a linear curve ($R^2 = 0.995$) is plotted over RIgG from 10 pg mL^{-1} to 100 ng mL^{-1}, demonstrating its potential applicability in real sample analysis. Table 1 lists a comparison between PBNP-based signal amplification method and previously reported ones in terms of analyte,

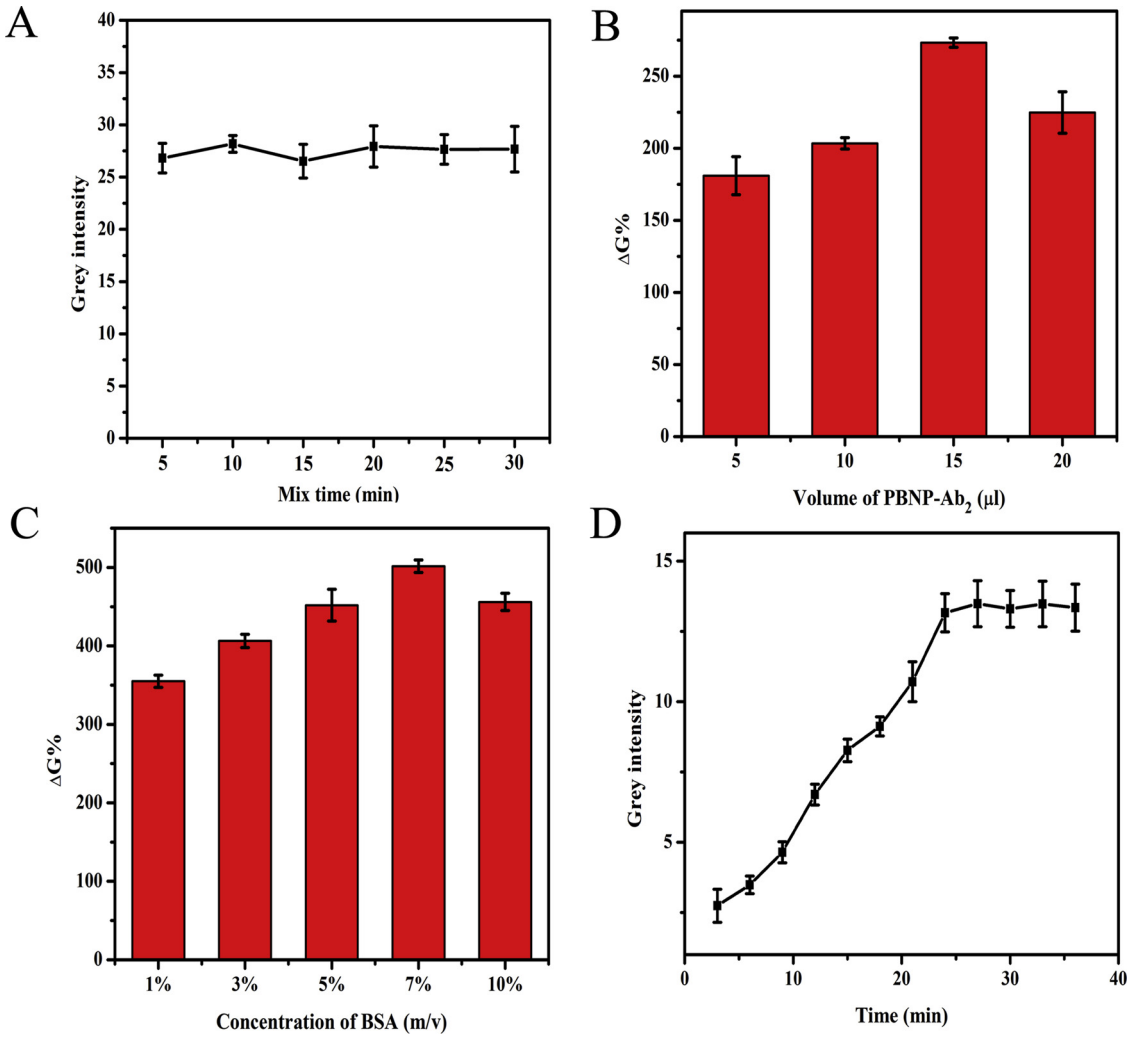

Fig. 3. Optimization of the experimental parameters. (A) Effect of analyte and PBNP-Ab_2pre-incubation time; (B) effect of PBNP-Ab_2 amount; (C) effect of BSA concentration in blocking reagent; (D) Time effect on color development of test band. Error bars show the standard deviation of three replicates.

detection limit and improvement efficiency. Average recovery(85 % - 99 %) and coefficient of variation (5 % - 15 %) were calculated by detection of RIgG at low (10^1 pg mL^{-1}), medium (10^3 pg mL^{-1}), and high level (10^5 pg mL^{-1}) in spiked serum, indicating reasonable accuracy and precision of this platform.

3.6. Feasibility of OTA detection

Theoretically, PBNP-LFIA can be easily adapted to detecting different analytes by simply changing antibody-antigen pairs. In order to evaluate universality of the proposed scheme, a small molecule

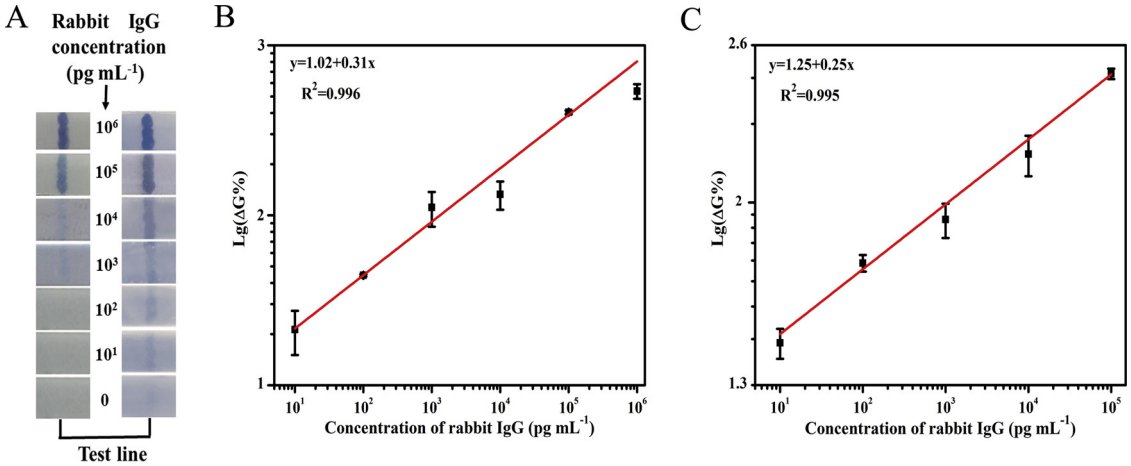

Fig. 4. (A) Photograph of the PBNP-LFIA strip for RIgG detection. Left：Before signal amplification; Right: After signal amplification. A linear relationship between the logarithmic of ΔG% and the concentration of RIgG in (B) PBS and (C) 10 % human serum. (n = 3).

Table 1
Effect of different signal amplification methods on the LFIA performance.

Signal amplification method	Analyte	LOD	Improvement	Ref.
Silver deposition	Abrin-a	0.1 ng mL^{-1}	100 fold	[25]
Gold deposition	*Escherichia coli O157:H7*	5×10^3 CFU mL^{-1}	8 fold	[26]
Enzyme catalyze	Human IgG	200 pg mL^{-1}	10 fold	[7]
Bifunctional AuNP	Procalcitonin	3 pg mL^{-1}	30 times	[27]
Combined with surface enhanced Raman spectroscopy	FluB	0.0085 μg mL^{-1}	1000 fold	[28]
Pt–Au bimetal NPs; TMB color development	*Escherichia coli O157:H7*	10^2 cell mL^{-1}	1000 fold	[29]
PBNP reporter/catalyze	Rabbit IgG	10 pg mL^{-1}	2–3 orders of magnitude	This work

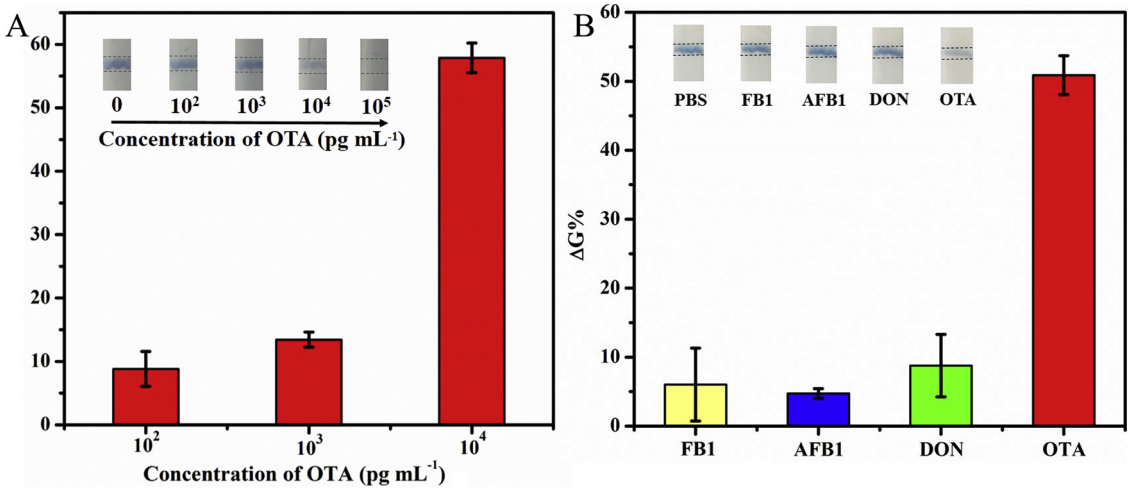

Fig. 5. OTA detection based on PBNP-LFIA strip. (A) OTA detection in soybeans extractives; (B) cross-reaction of the OTA strip to other common mycotoxins.

mycotoxin OTA was analyzed by the PBNP-LFIA strip based on a competitive immunoassay. When OTA is absent in the sample, PBNP-Ab_3 conjugate is captured by the OTA-BSA immobilized on the test line, resulting in a visual blue band. The excess conjugate moves continuously to the absorbent paper. However, if OTA is present in the sample, a part of binding sites on PBNP-Ab_3 are firstly occupied by the analytes OTA, forming a PBNP-Ab_3-OTA complex as a consequence. Thus, less PBNP-Ab_3 is captured at the test line, resulting in weaker signal intensity. With the increase of OTA concentration, more PBNP-Ab_3-OTA complex is formed, while less PBNP-Ab_3 is captured by OTA-BSA on the test line. Since the signal is negatively proportional to the analytes level in the competitive immunoassay, it is not necessary to amplify the signal with TMB. Soybean extractives spiked with different levels of OTA was analyzed with the proposed PBNP-LFIA platform. The highest signal intensity is observed from the negative control in Fig. 5 A.When OTA concentration increases from 100 pg mL^{-1} to 10 ng mL^{-1}, the intensity of the blue band becomes weaker and weaker, which can be differentiated by the naked eyes. However, the test line is completely disappeared at OTA concentration of 10 ng mL^{-1}. The histogram in Fig. 5A displays the quantitative results calculated according to the Eq. 2 in Section 2.6. $\Delta G_{OTA}\%$ is employed to indicate color change of the test line at each concentration as compared with the negative control. Based on the visual color and quantitative intensity, 100 pg mL^{-1} OTA in soybean extractives can be easily detected by the PBNP-LFIA strip, demonstrating its great application potential for fast and sensitive screening of mycotoxins in food safety supervision.

In order to further validate the OTA test specificity, three common mycotoxins FB1, AFB1 and DON were also analyzed with the PBNP-LFIA strip under identical conditions used for OTA test. As shown in Fig. 5B, ΔG% observed from OTA analysis is about 7–10 times higher than that from FB1, AFB1 and DON. Fig. 5B inset shows the images of test line for PBS (blank), FB1, AFB1, DON and OTA. The color of the test lines for FB1, AFB1 and DON is very similar to the blank group, while the color for OTA test becomes much lighter than PBS, indicating that only OTA induces a significant response. Thus, both the quantitative analysis and the color change clearly confirm the good specificity of the proposed PBNP-LFIA strip.

4. Conclusion

A low-cost, fast and sensitive LFIA strip is developed by using PBNP as a labeling tag instead of AuNP for signal generation and on demand cascade amplification. Signal generation is attributed to immunobinding-induced aggregation of the blue colored PBNP, while signal amplification is based on peroxidase-mimic PBNP-catalyzed TMB coloration. Under an optimal condition, a wide dynamic range from 10 pg mL^{-1} to 1 μg mL^{-1} and visual LOD of 10 pg $mL^{-1}$are obtained by the proposed PBNP-LFIA strip. Similar results are observed from detection of RIgG-spiked human serum. The LOD at 10 pg mL^{-1} is 2–3 orders of magnitude better than that achieved by the commercial AuNP-based LFIA strips. Furthermore, OTA in soybeans extractives is successfully detected by the PBNP-LFIA strip. In a word, the proposed platform is capable for fast and sensitive detection of biomacromolecules and small molecules in real samples.

Declaration of Competing Interest

The authors declare that they have no known competing financial interests or personal relationships that could have appeared to influence the work reported in this paper.

Acknowledgements

This work is financially supported by the National Key R&D Program of China (Grant 2017YFC1600900), National Natural Science Foundation of China (Grant 21475106), the Fundamental Research Funds for the Central Universities (Grant XDJK2018B004), Chongqing Engineering Research Center for Micro-Nano Biomedical Materials and

Devices, Southwest University, China.

References

[1] K. Zhang, S. Lv, Z. Lin, M. Li, D. Tang, Bio-bar-code-based photoelectrochemical immunoassay for sensitive detection of prostate-specific antigen using rolling circle amplification and enzymatic biocatalytic precipitation, Biosens. Bioelectron. 101 (2018) 159–166.

[2] R. Ren, G. Cai, Z. Yu, D. Tang, Glucose-loaded liposomes for amplified colorimetric immunoassay of streptomycin based on enzyme-induced iron(II) chelation reactionwith phenanthroline, Sensor. Actuator. B Chem. 265 (2018) 174–181.

[3] G. Liu, Y. Lin, J. Wang, H. Wu, C.M. Wai, Y. Lin, Disposable electrochemical immunosensor diagnosis device based on nanoparticle probe and immunochromatographic strip, Anal. Chem. 79 (2007) 7644–7653.

[4] L. Anfossi, C. Baggiani, C. Giovannoli, F. Biagioli, G. D'Arco, G. Giraudi, Optimization of a lateral flow immunoassay for the ultrasensitive detection of aflatoxin M1 in milk, Anal. Chim. Acta 772 (2013) 75–80.

[5] M. Xiao, K. Xie, X. Dong, L. Wang, C. Huang, F. Xu, W. Xiao, M. Jin, B. Huang, Y. Tang, Ultrasensitive detection of avian influenza A (H7N9) virus using surface-enhanced Raman scattering-based lateral flow immunoassay strips, Anal. Chim. Acta 1053 (2019) 139–147.

[6] T. Peng, J. Wang, S. Zhao, Y. Zeng, P. Zheng, D. Liang, G.M. Mari, H. Jiang, Highly luminescent green-emitting Au nanocluster-based multiplex lateral flow immunoassay for ultrasensitive detection of clenbuterol and ractopamine, Anal. Chim. Acta 1040 (2018) 143–149.

[7] C. Parolo, A.D.L. Escosura-Muñiz, A. Merkoçi, Enhanced lateral flow immunoassay using gold nanoparticles loaded with enzymes, Biosens. Bioelectron. 40 (2013) 412–416.

[8] D. Tang, J.C. Sauceda, Z. Lin, S. Ott, E. Basova, I. Goryacheva, S. Biselli, J. Lin, R. Niessner, D. Knopp, Magnetic nanogold microspheres-based lateral-flow immunodipstick for rapid detection of aflatoxin B2 in food, Biosens. Bioelectron. 25 (2009) 514–518.

[9] C. Liu, Q. Jia, C. Yang, R. Qiao, L. Jing, L. Wang, C. Xu, M. Gao, Lateral flow immunochromatographic assay for sensitive pesticide detection by using Fe3O4 nanoparticle aggregates as color reagents, Anal. Chem. 83 (2011) 6778–6784.

[10] J. Wang, L. Zhang, Y. Huang, A. Dandapat, L. Dai, G. Zhang, X. Lu, J. Zhang, W. Lai, T. Chen, Hollow Au-Ag nanoparticles labeled immunochromatography strip for highly sensitive detection of clenbuterol, Sci. Rep. 7 (2017) 41419.

[11] N. Grimaldi, F. Andrade, N. Segovia, L. Ferrer-Tasies, S. Sala, J. Veciana, N. Ventosa, Lipid-based nanovesicles for nanomedicine, Chem. Soc. Rev. 45 (2016) 6520–6545.

[12] G. Fu, W. Liu, S. Feng, X. Yue, Prussian blue nanoparticles operate as a new generation of photothermal ablation agents for cancer therapy, Chem. Commun. (Camb.) 48 (2012) 11567–11569.

[13] M. Hu, S. Furukawa, R. Ohtani, H. Sukegawa, Y. Nemoto, J. Reboul, S. Kitagawa, Y. Yamauchi, Synthesis of Prussian blue nanoparticles with a hollow interior by controlled chemical etching, Angew. Chem. 51 (2012) 984–988.

[14] M. Shatruk, A. Dragulescu-Andrasi, K.E. Chambers, S.A. Stoian, E.L. Bominaar, C. Achim, K.R. Dunbar, Properties of Prussian blue materials manifested in molecular complexes: observation of cyanide linkage isomerism and spin-crossover behavior in pentanuclear cyanide clusters, J. Am. Chem. Soc. 129 (2007) 6104–6116.

[15] H. Chen, Y. Ma, X. Wang, Z. Zha, Multifunctional phase-change hollow mesoporous Prussian blue nanoparticles as a NIR light responsive drug co-delivery system to overcome cancer therapeutic resistance, J. Mater. Chem. B 5 (2017) 7051–7058.

[16] Z. Qin, Y. Li, N. Gu, Progress in applications of Prussian blue nanoparticles in biomedicine, Adv. Healthcare Mater. 7 (2018) e1800347.

[17] X. Zhang, S.W. Gong, Y. Zhang, T. Yang, C.Y. Wang, N. Gu, Prussian blue modified iron oxide magnetic nanoparticles and their high peroxidase-like activity, J. Mater. Chem. 20 (2010) 5110–5116.

[18] W. Zhang, D. Ma, J. Du, Prussian blue nanoparticles as peroxidase mimetics for sensitive colorimetric detection of hydrogen peroxide and glucose, Talanta 120 (2014) 362–367.

[19] V. Čunderlová, A. Hlaváček, V. Horňáková, M. Peterek, D. Němeček, A. Hampl, L. Eyer, P. Skládal, Catalytic nanocrystalline coordination polymers as an efficient peroxidase mimic for labeling and optical immunoassays, Microchim. Acta 183 (2016) 651–658.

[20] Z. Farka, V. Cunderlova, V. Horackova, M. Pastucha, Z. Mikusova, A. Hlavacek, P. Skladal, Prussian blue nanoparticles as a catalytic label in a sandwich nanozyme-linked immunosorbent assay, Anal. Chem. 90 (2018) 2348–2354.

[21] M. Shokouhimehr, A.K.Eric S. Soehnlen, S. Basu, S.D. Huang, Biocompatible Prussian blue nanoparticles: preparation, stability, cytotoxicity, and potential use as an MRI contrast agent, Inorg. Chem. Commun. 13 (2010) 58–61.

[22] M. Shokouhimehr, Eric S. Soehnlen, J. Hao, M. Griswold, C. Flask, X. Fan, James P. Basilion, S. Basu, S.D. Huang, Dual purpose Prussian blue nanoparticles for cellular imaging and drugdelivery: a new generation of T1-weighted MRI contrast and small moleculedelivery agents, J. Mater. Chem. 20 (2010) 5251–5259.

[23] M. Tian, L. Lei, W. Xie, Q. Yang, C.M. Li, Y. Liu, Copper deposition-induced efficient signal amplification for ultrasensitive lateral flow immunoassay, Sensor. Actuator. B Chem. 282 (2019) 96–103.

[24] B. Zhao, Q. Huang, L. Dou, T. Bu, K. Chen, Q. Yang, L. Yan, J. Wang, D. Zhang, Prussian blue nanoparticles based lateral flow assay for high sensitive determination of clenbuterol, Sensor. Actuator. B Chem. 275 (2018) 2223–2229.

[25] W. Yang, X.B. Li, G.W. Liu, B.B. Zhang, Y. Zhang, T. Kong, J.J. Tang, D.N. Li, Z. Wang, A colloidal gold probe-based silver enhancement immunochromatographic assay for the rapid detection of abrin-a, Biosens. Bioelectron. 26 (2011) 3710–3713.

[26] J. Wang, M. Chen, Z. Sheng, D. Liu, S. Wu, W. Lai, Development of colloidal gold immunochromatographic signal-amplifying system for ultrasensitive detection of Escherichia coli O157:H7 in milk, RSC Adv. 5 (2015) 62300–62305.

[27] N.A. Taranova, A.E. Urusov, E.G. Sadykhov, A.V. Zherdev, B.B. Dzantiev, Bifunctional gold nanoparticles as an agglomeration-enhancing tool for highly sensitive lateral flow tests: a case study with procalcitonin, Microchim. Acta 184 (2017) 4189–4195.

[28] I.H. Cho, M. Das, P. Bhandari, J. Irudayaraj, High performance immunochromatographic assay combined with surface enhanced Raman spectroscopy, Sensor. Actuator. B Chem. 213 (2015) 209–214.

[29] T. Jiang, Y. Song, T. Wei, H. Li, D. Du, M.J. Zhu, Y. Lin, Sensitive detection of Escherichia coli O157:H7 using Pt–Au bimetal nanoparticles with peroxidase-like amplification, Biosens. Bioelectron. 77 (2016) 687–694.

Meiling Tian received her bachelor degree in bioengineering from Northwest A&F University, Shanxi province, China in July 2016. She currently is a master student majoring in analytical chemistry at Southwest University, Chongqing. Her research focuses on development and applications of immunoassay test strip.

Wenyue Xie obtained her bachelor degree in chemistry in 2016. She currently is a master student majoring in analytical chemistry at Southwest University, Chongqing, China. Her research interests are nanomaterials-based colorimetric biosensors and their applications.

Ting Zhang received her bachelor degree in agriculture from Xichang College, Sichuan province, China in July 2018. In September 2018, she was enrolled as a master student in Institute for Clean Energy & Advanced Materials, Southwest University, Chongqing, China. Her research work focuses on development and applications of immunoassay test strip.

Yang Liu received his Bachelor Degree in Agronomy from Northeast Forestry University in 1987, his Master Degree from the University of Goettingen, in 1999, his PhD from the University of Hohenheim in 2004 and worked as a Post Doc in the Institute of Phytomedicine, University of Hohenheim, Germany in 2005. Since 2006 he worked in the Institute of Science and Technology, Chinese Academy of Agricultural Sciences (CAAS). Prof. Liu' research focuses on prevention and control of agro-products processing hazards. He is currently the chief scientist of the National Key R&D Program of China. He also serves as the editor-in-chief of Journal of Microbiology and Biotechnology Research, editor-in-charge of International Journal of Clinical Microbiology and Biochemical Technology, guest editor of Food Additives & Contaminants: Part A and Toxins, and editorial board member for other 7 international scientific journals.

Zhisong Lu received his PhD degree in school of chemical & biomedical engineering from Nanyang Technological University, Singapore in 2011, and is currently a professor in Faculty of Materials & Energy, Southwest University, P. R. China. Prof. Lu's research expertise is in functional nanomaterials and biosensors. With an h-index of 33 and total citation of 3400, he has co-authored more than 130 papers in refereed journals and has filed 11 patents. He also serves as an advisory board member of Fundamental Toxicological Sciences.

Chang Ming Li received a doctorate from Wuhan University in 1986. He has been working at Nanyang Technological University in Singapore since 2003. He once served as lifelong professor of Nanyang Technological University, director of the Department of Bioengineering, and director of the Center for Advanced Nanosystems. Prof. Li was selected as Academician by the American Academy of Medical Sciences in 2010. At the same time, Prof. Li is also a Fellow of the Royal Society of Chemistry and a Special Professor of the National "Thousand Talents Program." From January 2012 to the present, he served as dean of Clean Energy & Advanced Materials, Southwest University. Prof. Li's research focuses on clean energy (fuel cells, solar cells, and lithium-ion batteries) and advanced materials (nanomaterials, energy materials, biomaterials, and chemical/biosensor materials).

Yingshuai Liu completed his doctorate in School of Chemical and Biomedical Engineering at Nanyang Technological University (Singapore) in 2011. After a short post-doctoral training in same group, Dr. Liu joined Institute for Clean Energy and Advanced Materials at Southwest University as an associate professor. He has been promoted to a full professor in 2017. Dr. Liu's group works on interdisciplinary research topics including design and synthesis of functional nanomaterials and development of novel nanomaterials-based biosensors/biochips for applications in fundamental biology, biomedical diagnosis, and food safety. He has published more than 50 peer-reviewed papers in international journals.